AIAA JOURNAL
Vol. 33, No. 1, January 1995

Aeroacoustic Model for Weak Shock Waves Based on Burgers Equation

Sanford S. Davis*
NASA Ames Research Center, Moffett Field, California 94035-1000

The adiabatic form of the Euler equations are cast in a form emphasizing its signal propagation properties and solved using an approximate eigenfunction analysis. Second-order rarefaction waves appear as direct eigenfunction solutions. The underlying scalar equation describing nonlinear shock wave evolution is rederived as a first-order Burgers equation. The characteristic sonic boom *N* waves are predicted using an implicit aeroacoustic-based finite-difference algorithm with numerical damping designed to suppress spurious oscillations at shock-wave discontinuities. The evolution of these sonic-boom-type signals to the mid- and far field are computed directly with the numerical method.

Nomenclature

a	= speed of sound
Cn	= equivalent Courant number used in numerical analysis
Dn_2, Dn_4	= damping constants for numerical dissipation
$\boldsymbol{G}$	= eigenvector
k	= wavenumber, 2π/wavelength
M	= freestream Mach number
p	= pressure
R	= log density
$\boldsymbol{u}$	= vector of dependent variables, $[R, u, v, p]$
u, v	= axial and vertical velocities
u', v'	= perturbation velocities normalized by a_{inf}
x, y	= Cartesian coordinates
β	= $\sqrt{M^2-1}$
γ	= ratio of specific heats, c_p/c_v
Δx, Δy, Δt	= step size in x, y, and time
$\Delta\xi$, $\Delta\eta$	= step size in oblique coordinate system
λ	= eigenvalue
ρ	= density
$()_{\text{inf}}$	= Reference to freestream conditions
$()^*$	= Reference to a physical quantity

Introduction

SONIC boom prediction is an important application of weak shock-wave theory. The state of the art has evolved from the analysis of long-range propagation of weak disturbances[1-3] to parametric studies of geometrically complex aircraft-type configurations. Older methods were based on studies of weak disturbances consisting of a simple distribution of sources and sinks to represent aircraft components.[4] Previous sonic-boom studies in this zone represented the wing-body-tail as a simple area distribution. Sonic-boom analysis is now considered a three-zone problem.[5] The first zone is bounded by the vehicle and a near-field control surface. The flow in this region is very intricate and requires complicated Euler or even Navier-Stokes solvers since detailed and irregular boundary conditions must be satisfied. The second zone is a kind of buffer region bounded by two control surfaces. An inner surface coupling to the body flowfield and an outer surface interfacing with the ray theory region. In this intermediate zone, one would like to compute the flow with higher fidelity than the ray region, but without the physical complexity of the inner zone. It is also desirable to place the inner boundary as close as possible to the body. The third zone is the classical ray region where wind, temperature, and turbulence are accounted for as one-dimensional flow along a ray tube to the ground.[6]

This paper solves a simplified system of equations governing the second zone in a two-dimensional context. An approximate eigenfunction expansion and its associated Burgers equation capture the important physics of the velocity and pressure fields to second order. The aerodynamics literature of the 1940s and 1950s introduced certain ad hoc approximations to the exact potential flow for high-speed flows. One such approximation, as outlined, for example, in Ref. 7, is a second-order quasilinear hyperbolic PDE that is essentially equivalent to the one derived here. A similar second-order PDE was formally worked out from perturbation theory in Ref. 8. These second order PDEs possess two characteristics, one of which is primary for shock-wave propagation. The derivation presented here shows how a first-order scalar Burgers equation with the one dominant characteristic emerges from the eigenfunction analysis and can be used to construct a complete second-order approximation to the steady supersonic aerodynamics problem. Such Burgers models have been known for some time in the analysis of nonlinear acoustic problems, e.g., Ref 8. This solution is also compatible with nonlinear simple wave theory[9] to this order.

A numerical solution to the aerodynamic Burgers equation is computed with the same implicit finite-difference algorithm originally applied to acoustics.[10] This simple method is augmented with a mixture of second- and fourth-order numerical damping to suppress the troublesome oscillations that usually accompany discontinuous solutions. These oscillations can mask the far-field sonic-boom N waves.

Solutions for the two-dimensional shock-wave problem in the midfield are illustrated for an airfoil that generates multiple shock waves. A comparison among three different airfoil sections confirm the similarity law regarding N waves far away from the emitting body. The slope of the N wave is independent of airfoil shape, but the precise fore and aft shock-wave location along the spine of the N depends on the source geometry.

Equations of Motion and Eigenfunction Analysis

The steady-state Euler equations of mass and momentum conservation for a compressible gas in terms of the physical kinematic and thermodynamic quantities u^*, v^*, p^*, and ρ^* are

$$u^*\frac{\partial\rho^*}{\partial x^*}+v^*\frac{\partial\rho^*}{\partial y^*}+\rho^*\frac{\partial u^*}{\partial x^*}+\rho^*\frac{\partial v^*}{\partial y^*}=0$$

$$u^*\frac{\partial u^*}{\partial x^*}+v^*\frac{\partial u^*}{\partial y^*}+\frac{1}{\rho^*}\frac{\partial p^*}{\partial x^*}=0$$

$$u^*\frac{\partial v^*}{\partial x^*}+v^*\frac{\partial v^*}{\partial y^*}+\frac{1}{\rho^*}\frac{\partial p^*}{\partial y^*}=0$$

Received March 7, 1994; revision received Aug. 20, 1994; accepted for publication Aug. 24, 1994.

*Chief, Fluid Mechanics Laboratory Branch. Associate Fellow AIAA.

Isentropic flow in air assumes a relation between density and pressure of the form $p(\rho) = \text{const}\,\rho^{\gamma}$ where γ is the ratio of specific heats c_p/c_v. In addition, the local speed of sound is defined by the thermodynamic derivative $\mathrm{d}p^*/\mathrm{d}\rho^* = \gamma p^*/\rho^* = a^{*2}$. To emphasize the two-dimensional propagation character of the equation, choose a new dependent variable $R = \log(\rho^*)$ so that all coefficients become velocities. The final equations of motion for a compressible, adiabatic fluid are

$$\begin{aligned} u^*\frac{\partial R}{\partial x^*} + v^*\frac{\partial R}{\partial y^*} + \frac{\partial u^*}{\partial x^*}\frac{\partial v^*}{\partial y^*} &= 0 \\ a^{*2}\frac{\partial R}{\partial x^*} + u^*\frac{\partial u^*}{\partial x^*} + v^*\frac{\partial u^*}{\partial y^*} &= 0 \\ a^{*2}\frac{\partial R}{\partial y^*} + u^*\frac{\partial v^*}{\partial x^*} + v^*\frac{\partial v^*}{\partial y^*} &= 0 \end{aligned} \tag{1}$$

These equations are equivalent to the well-known nonlinear potential flow equations but are retained as a first-order system to facilitate eigenfunction analysis. It is convenient to express the dependent variables in terms of the free stream speed of sound a_{inf}. Thus, $u^* = a_{\text{inf}}(M + u')$, $v^* = a_{\text{inf}}v'$, $a^* = a_{\text{inf}}a$ where M is the freestream Mach number. The final equation in matrix-vector form is

$$\begin{bmatrix} M+u' & 1 & 0 \\ a^2 & M+u' & 0 \\ 0 & 0 & M+u' \end{bmatrix} \frac{\partial}{\partial x}\begin{bmatrix} R \\ u' \\ v' \end{bmatrix} + \begin{bmatrix} v' & 0 & 1 \\ 0 & v' & 0 \\ a^2 & 0 & v' \end{bmatrix} \frac{\partial}{\partial y}\begin{bmatrix} R \\ u' \\ v' \end{bmatrix} = 0 \tag{2}$$

and the solution vector is $\boldsymbol{u} = [R, u', v']^T$. Let us quickly analyze the solution for linear supersonic flow: u' and v' are deleted from the coefficient matrices, and the speed of sound is set to unity. The dependent variable x is considered a time-like variable. The acoustic analogy is complete if the inverse of the first matrix is multiplied through to obtain the simplified form $\partial \boldsymbol{u}/\partial x + A\partial \boldsymbol{u}/\partial y$. The acoustic-analog equation is

$$\frac{\partial}{\partial x}\begin{bmatrix} R \\ u' \\ v' \end{bmatrix} + \begin{bmatrix} 0 & 0 & \dfrac{M}{\beta^2} \\ 0 & 0 & -\dfrac{1}{\beta^2} \\ \dfrac{1}{M} & 0 & 0 \end{bmatrix} \frac{\partial}{\partial y}\begin{bmatrix} R \\ u' \\ v' \end{bmatrix} = 0 \tag{3}$$

where $M, \beta = \sqrt{M^2 - 1}$ are constant depending only on freestream conditions. This system is easy to solve. One way is to assume a uniformly propagating wave solution of the form $\boldsymbol{u} = f(x - y/\lambda)\boldsymbol{G}$ with λ an undetermined constant and $\boldsymbol{G}$ its associated eigenvector. The general solution of the eigenvalue problem in terms of arbitrary functions f, g, and h is

$$\mathbf{u} = \begin{bmatrix} 0 \\ 1 \\ 0 \end{bmatrix} f(y) + \begin{bmatrix} -M/\beta \\ 1/\beta \\ 1 \end{bmatrix} g(x + \beta y) + \begin{bmatrix} M/\beta \\ -1/\beta \\ 1 \end{bmatrix} h(x - \beta y) \tag{4}$$

Of the three terms, the first two are disregarded on physical grounds. (Using the wave system in the first quadrant, the two disregarded eigenvalues are 0 and $-1/\beta$.) What remains is the Ackeret solution for linear supersonic aerodynamics, where the function h is proportional to the local airfoil slope, e.g., $h(x) = MY'(x)$. The relationship among the linear solutions (to be used in the nonlinear analysis) is $\beta u' + v' = 0$ and $\beta R - Mv' = 0$.

Now consider solutions to the complete perturbed Euler equations of Eq. (2). The first-order speed of sound from Bernoulli's equation is $a^2 = 1 - (\gamma - 1)Mu'$. Solutions are again sought in the eigenvector form $\boldsymbol{u} = f(x - y/\lambda)\boldsymbol{G}$. The approximate Euler equation admits nontrivial solutions for certain values of λ determined from $\mathrm{Det}[A - \lambda A'] = 0$ where coefficient matrices A and A' are those of Eq. (2). From linear analysis the three eigenvalues are $1/\beta$, $-1/\beta$, and 0. Here we will search for eigenvalues of the form $1/\beta + \varepsilon$. The small quantity ε involves the perturbation velocities u', v', and the log density R.

The analysis follows by solving the cubic eigenvalue equation to first order in small quantities. The values v' and R are taken from linear theory. After considerable algebra, the result is

$$\lambda = \frac{1}{\beta} - \frac{(\gamma+1)M^3}{2\beta^3}u' = \frac{1}{\beta} + \frac{(\gamma+1)M^4}{2\beta^4}\frac{v^*}{U_{\text{inf}}} \tag{5}$$

which matches the slope of the local Mach line to second order as given, for example, in Ref. 11.

Using the eigenfunction analog, we can go a step further and compute the eigenvector $\boldsymbol{G}$. The eigenvector follows from the second and third of the perturbed Euler equations

$$\mathbf{G}\cdot v' = \begin{bmatrix} R \\ u' \\ v' \end{bmatrix} = \begin{bmatrix} \dfrac{Mv'}{\beta} + \dfrac{M^2(M^2 + 2\gamma - M^2\gamma)v'^2}{2\beta^4} \\ -\dfrac{v'}{\beta} - \dfrac{M^3(\gamma+1)v'^2}{2\beta^4} \\ v' \end{bmatrix} \tag{6}$$

This is a second-order local approximation to the adiabatic Euler equations. Given one dependent variable (here v'), the other two may be computed directly from Eq. (6). This expression is confirmed with published formulas from simple wave theory. For example, the relation between $C_p = (p - p_{\text{inf}})/\frac{1}{2}\rho_{\text{inf}}U_{\text{inf}}^2$ and the local flow deflection angle θ is found by manipulating Eq. (6) into

$$C_p = \frac{2}{\beta}\theta + \frac{(M^2-2)^2 + \gamma M^4}{2\beta^4}\theta^2 \tag{7}$$

which matches the approximation given in Ref. 11.

The governing nonlinear PDE is obtained by assuming that f is not a plane wave but a general function of x and y so that $\partial f/\partial x + \lambda \partial f/\partial y = 0$. Even though the approximate solution for rarefaction waves is already given by Eq. (6), the PDE is best for computing overlapping compression waves and evolving shocks. It is well known that such equations are archetypes for nonlinear waves. The function f is the vertical velocity v' and can be solved as a boundary value problem with a well-defined boundary condition—the local slope of an airfoil. This solution is the first step in the two-step process of solving the adiabatic Euler equations. The remaining step is to compute dependent variables from the local characteristic form in Eq. (6).

Since there are only two independent variables it is irrelevant which is the "time" or evolving coordinate. It is most useful in shock propagation problems to march perpendicular to the flow, and the final second-order equation is

$$\frac{\partial v'}{\partial y} + \beta\frac{\partial v'}{\partial x} - \frac{M^3(\gamma+1)v'}{2\beta^2}\frac{\partial v'}{\partial x} = 0 \tag{8}$$

The boundary value is completed by specifying the upwash on the inner control surface. For thin airfoil analysis the curve representing the airfoil is $y = Y(x)$ and $v'(x, 0) = MY'(x)/[1 + Y'(x)/\beta]$ to second order.

Numerical Solutions

The computational method consists of a two-step sequence. Consider a uniform grid with spacing Δx and Δy. If a dependent variable

$u(x, y) = u(j\Delta x, n\Delta y)$ is denoted by u_j^n, the locally frozen dependent variable defines an equivalent Courant number

$$Cn = \left(\beta - \frac{M^3(\gamma+1)u_j^n}{2\beta^2}\right)\frac{\Delta y}{\Delta x}$$

This quantity enters as a parameter in the following two-time level, three-point neutrally stable implicit scheme[10]:

$$(Cn-1)(Cn-2)u_{j-1}^{n+1} - 2(Cn-2)(Cn+2)u_j^{n+1} + (Cn+1)(Cn+2)u_{j+1}^{n+1} = (Cn+1)(Cn+2)u_{j-1}^n - 2(Cn-2)(Cn+2)u_j^n + (Cn-1)(Cn-2)u_{j+1}^n \quad (9)$$

Equation (9) is formally fourth-order accurate in space and time for a globally constant Courant number. Good resolution may be obtained with values of the parameter Cn up to 2 if the governing equations were linear with constant coefficients.

This first computational step will propagate all wave numbers from level y to $y + \Delta y$ up to the grid imposed limit $k_{\max} = 2\pi/2\Delta x = \pi/\Delta x$. The nondimensional quantity $k\Delta x$, which varies from 0 to π, plays a key role in the analysis of finite-difference methods.[12] Since the scheme is neutrally stable (no numerical dissipation) short waves will not damp causing nonphysical oscillations in regions of large flow gradients. Lower order upwind methods possess built-in algorithm-induced damping which alleviates this effect but may suffer in solution accuracy.

The second part of the sequence is a damping step consisting of second- and fourth-order terms with damping constants Dn_2 and Dn_4

$$(Dn_2 + 12Dn_4)u_{j-1}^{n+1} + (10Dn_2 - 24Dn_4)u_j^{n+1} + (Dn_2 + 12Dn_4)u_{j+1}^{n+1} = \left(Dn_2 + 12Dn_2^2 + 12Dn_4\right)u_{j-1}^n + \left(10Dn_2 - 24Dn_2^2 - 24Dn_4\right)u_j^n + \left(Dn_2 + 12Dn_2^2 + 12Dn_4\right)u_{j+1}^n \quad (10)$$

The algorithm is equivalent to a Crank-Nicolson scheme for the heat equation if $Dn_4 = 0$. The full algorithm is equivalent to the parabolic PDE $u_t = Dn_2\Delta x^2 u_{xx} + Dn_4\Delta x^4 u_{xxxx}$. Values of $Dn_2 = 0.01$ and $Dn_4 = 0.0013$ were found adequate for this application. This is less damping than that induced by simple upwind methods which is the order $Dn_2 = Cn/2$.

An unsteady Burgers equation is commonly used to illustrate nonlinear wave motion. A particularly simple sine wave initial condition, $u(x, 0) = \sin(x)$ $0 > x > 2\pi$ nicely illustrates the problem of numerical wave dispersion since high wave numbers are generated as part of the nonlinear evolution process. Burgers equation solutions to the model problem are computed in Fig. 1. The equation is $u_t + uu_x = 0$ subject to the sine wave initial condition mentioned earlier. Exact analytical solutions are available to the time that a discontinuity first forms at $t = 1.47$ s. The algorithm described was used on a 125-point mesh with a maximum Courant number $u_{\max}\Delta\tau/\Delta x = 0.2$ and damping values indicated previously. The time lagged value of $u(x, t)$ was used to compute the local Courant number. Solutions to Eqs. (9) and (10) require inversion of a tridiagonal matrix at each time step.

The curves in Fig. 1 show that the exact solution (dashed) is almost coincident with the numerical solution (solid) at four times to $t = 1.47$ s. The maximum error between the exact and numerical solution at $t = 1.47$ s is 0.7%. The second-step damping is sufficient to suppress the oscillations but not enough to compromise the sharp discontinuity. (Numerical experiments using first-order upwind methods showed a comparable error of 3.3% with an equivalent damping of $Cn_{\max}/2 = 0.1$. Some computations with second-order methods approximately halved the latter error.) Highly accurate solutions to this model problem can also be found in the literature using locally adaptive grids, spectral methods,[13] and combinations of the two.[14] These methods involve elegant algorithmic constructions.

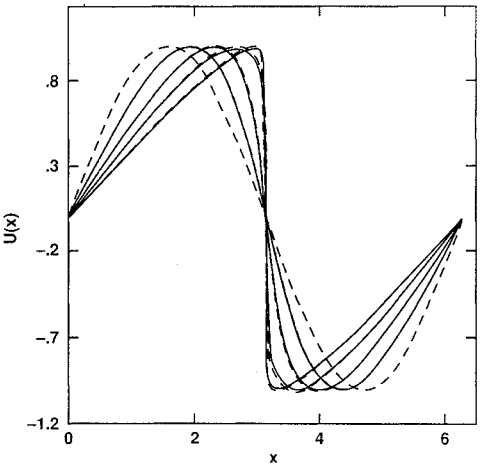

Fig. 1 Comparison of analytical and numerical solutions to Burgers equation subject to a sine wave initial condition to the instant where a discontinuity first forms at $t = 1.47$ with s second- and fourth-order damping constants 0.01 and 0.0013, respectively, and $N = 125$ mesh points.

The fidelity of the scheme in terms of wave number resolution is shown in Fig. 2. The upper right panel (Fig. 2b) shows the Fourier wave number spectrum for the final signal of Fig. 1, which is repeated in Fig. 2a. The harmonic content of this highly distorted sine wave decays at a relatively low rate. This gradual decay is an indication that short waves are important contributors to the discontinuous waveform. The wave in the lower left (shown in Fig. 2c from another calculation with marginal damping) indicates incipient instability. Subcritical damping allowed numerical dispersion to adversely affect the resolution of high wave numbers. This low damping causes a spectral upsweep at higher wave numbers as shown in Fig. 2d. Adequate damping effectively eliminates this fatal upsweep. Of course, the appropriately damped case in the upper row must have some physical effect on the wave, and slight smoothing of the shoulders is apparent in the signal. A problematic aspect of this approach is that there is no universal best damping, but one may be matched to signals possessing a certain class of spectra. It must be emphasized that these effects are not due to nonlinearities, but are the cumulative effect of applying consistant discrete approximations to the partial differential equations over a large number of time steps.

Next, consider the evolution of a type of N wave. Numerical and analytical solutions for an approximate N wave are shown in Fig. 3. Numerical solutions are compared with the exact solution to Burgers equation given, for example, in Ref. 15 as

$$u(x,t) = \frac{x}{t}\left\{1 + \sqrt{\frac{t}{10}\frac{e^{x^2/0.05t}}{e^{20}-1}}\right\}^{-1}; \qquad t \geq 10 \quad (11)$$

The analytical solution at $t = 10$ and $t = 24$ are shown as dashed lines in Fig. 3. The computed curve at $t = 24$ (723 time steps) is also indicated. A number of parametric studies indicate that the main (but significant) effect of lagging the nonlinear term is to limit the allowable time step to 20% or less than that which one would otherwise use for a strictly linear, constant-coefficient problem (that is, a Courant number of a few tenths rather than unity).

Steady supersonic flow is now considered. A preliminary transformation to semioblique coordinates fixes the shock waves relative to the primary linear characteristic. In the new coordinate system $\xi = x - \beta y$, $\eta = y$ Eq. (8) becomes a Burgers equation

$$\frac{\partial v'}{\partial \eta} - \frac{M^3(\gamma+1)v'}{2\beta^2}\frac{\partial v'}{\partial \xi} = 0 \quad (12)$$

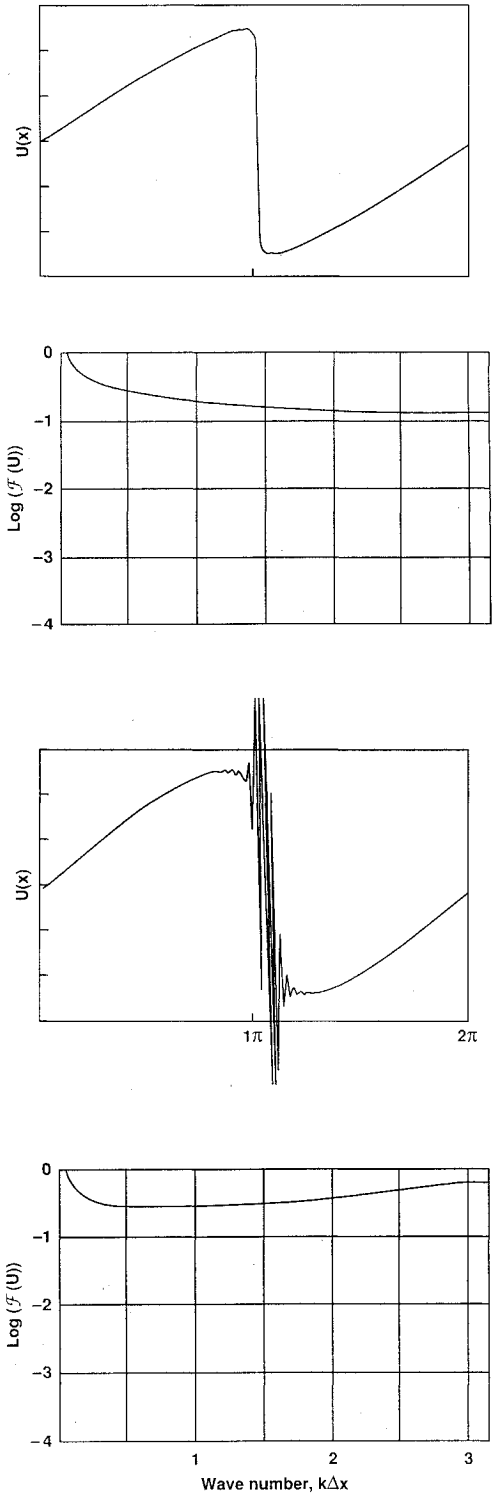

Fig. 2 Fourier analysis of a discontinuous signal: a) final signal from Fig. 1, b) Fourier spectrum, c) typical signal just before instability, and d) Fourier spectrum.

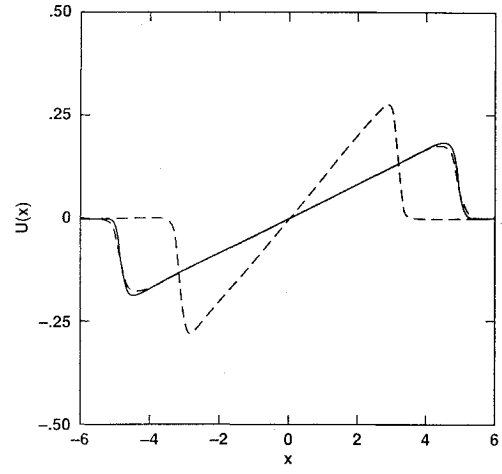

Fig. 3 Comparison between numerical and analytical solution for an approximate N wave, initial time = 10, final time = 24, N = 125, $\Delta t/h$ = 0.2, solution after 723 time steps: ----- analytical solution and —— numerical solution.

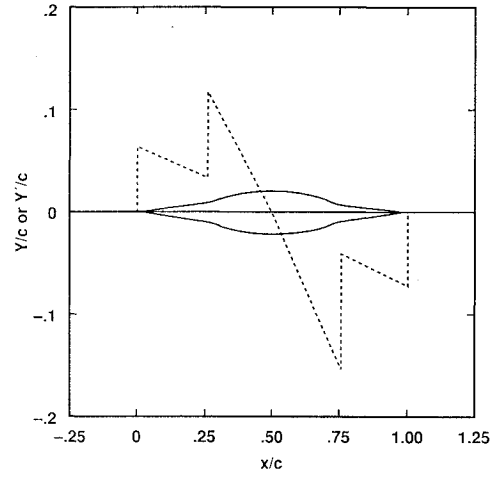

Fig. 4 Bicircular arc airfoil contour and slope distribution.

and the relevant Courant number is

$$Cn = -\frac{M^3(\gamma+1)v_j'^n}{2\beta^2}\frac{\Delta\eta}{\Delta\xi}$$

at $v'(\xi,\eta) = v'(j\Delta\xi, n\Delta\eta)$.

A model for a multiple-shocked airfoil is the bicircular arc shown in Fig. 4. The profile is shown along with a chordwise slope distribution (shown as a dashed line) which is proportional to the linear pressure. Four shocks appear at the slope discontinuities as indicated. The airfoil is 4.2% thick and the second-order corrections to the density and axial velocity in Eq. (6) were insignificant. Equation (12) was solved numerically using the two-step algorithm with the indicated boundary values as initial conditions.

Solutions are presented in Figs. 5 and 6 to show the effect of damping on the evolution of N waves. Over 2000 steps in y (time steps) were taken to obtain pressure signatures to a vertical distance of approximately 20 chords. After propagating a few chords, the multiple shocks merge into a single N wave that decays in a universal manner. This is the near- and far-field region discussed in the Introduction. The effect of damping is complementary, near-field overshoots (lower part of Fig. 5a) with low damping evolved into well-formed N waves. Higher damping caused well-formed N waves in the near field (lower part Fig. 5b) that evolved into slightly dissipated waves farther out.

A comparison of the far-field signatures at $y/c = 19.5$ is shown in Fig. 6. The undistorted linear wave is shown as a dashed line to indicate the nonlinear evolution. The evolved wave has spread, decreased in magnitude, and merged into a front and rear shock. The N wave has lost all information regarding the detailed airfoil geometry. (Linear theory always remembers each and every detail of the emitting airfoil.) The N wave gradient, a universal feature of these signals, is exactly the same. The only effect of damping is slight shock wave smoothing at $Dn_2 = 0.03$. Other computations using over 20,000 time steps (to a few hundred chords) showed that

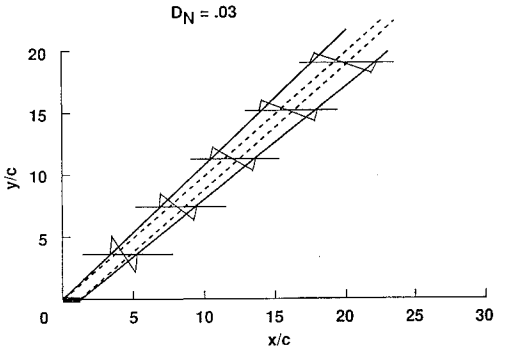

a)

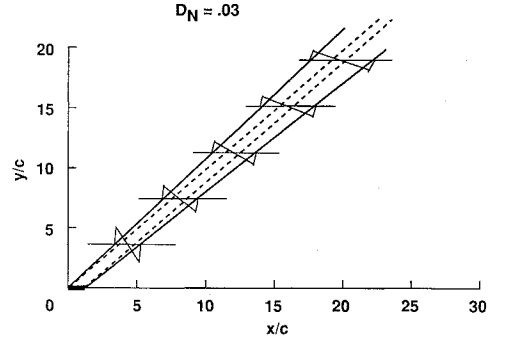

b)

Fig. 5 Shock-wave patterns for a bicircular arch airfoil; 250 points centered about linear characteristics, 2000 steps to y = 19.3c, Mach number = 1.414: a) damping Dn_2 = 0.01 and b) damping Dn_2 = 0.03.

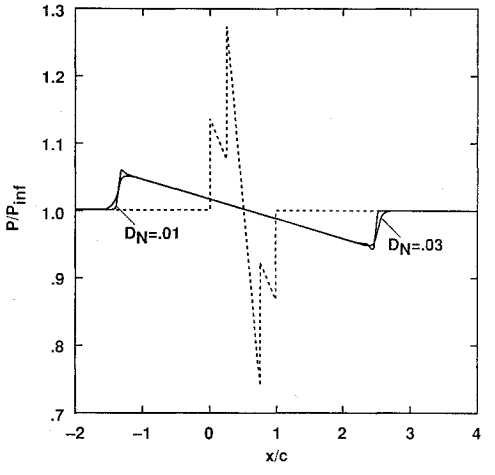

Fig. 6 Shock wave at y = 19.3c showing effect of damping on the fidelity of the N wave, dashed line shows linearized pressure distribution.

the N wave slope decays at a universal rate that is an inverse first power of the altitude y.

Figure 7 compares signatures in the near-field region with linear theory, again shown as dashed lines. Four signatures are shown at increasing altitudes in Figs. 7a–7d. There is a rapid merging of shocks and quick decay (greater than y^{-1}) until the N wave first forms at a distance slightly greater than 1.16c. The wave ultimately decays at its asymptotic rate. These two-dimensional flows form mature N waves quite rapidly.

The effect of geometry on the midfield shock wave is investigated with the three airfoil sections shown in Fig. 8. The first section is the bicircular arc considered previously. The other two airfoils are a 5% circular arc and a cusped airfoil. The former starts with an N wave and the latter with a continuous shockless pressure distribution. The N waves at y/c = 19.5 are shown in Fig. 9. As expected, the slope is independent of geometry; but an interesting result is

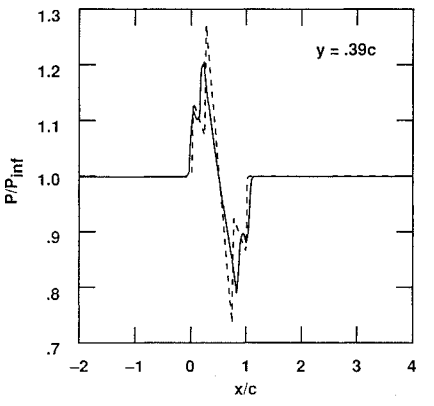

a)

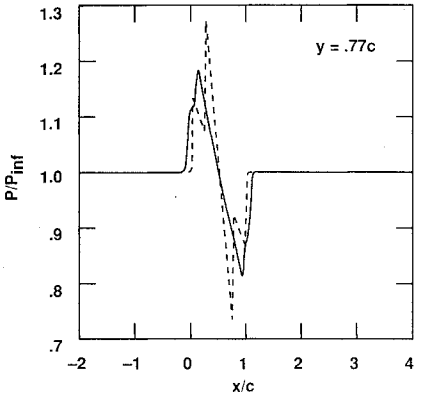

b)

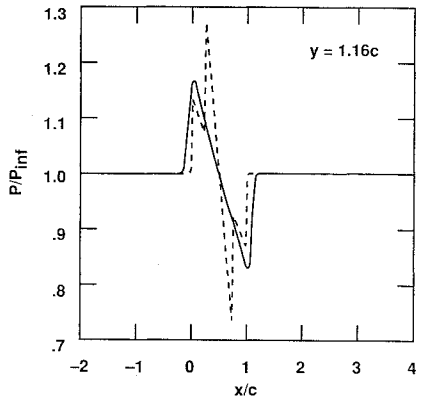

c)

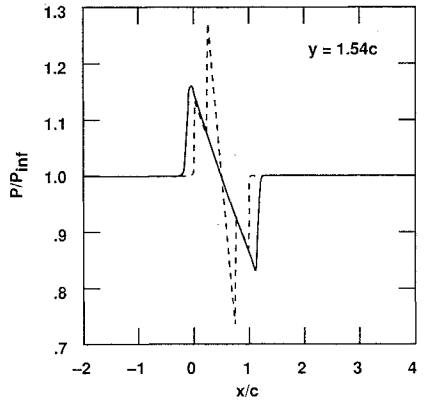

d)

Fig. 7 Evolution of a multishock system into a single N wave in the near field, dashed lines show linear pressures: a) y = 0.39c, b) y = 0.77c, c) y = 1.16c, and d) y = 1.54c.

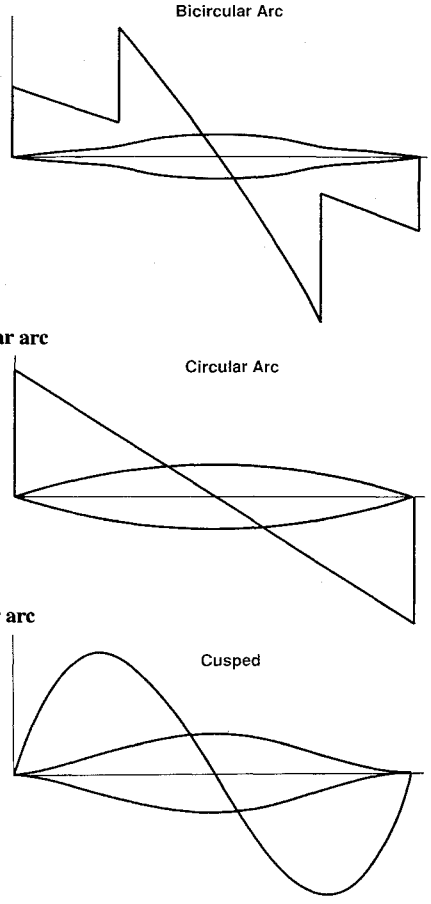

Fig. 8 Geometry and initial pressure distribution of investigated airfoils: bicircular arc, circular arc, and cusped airfoil.

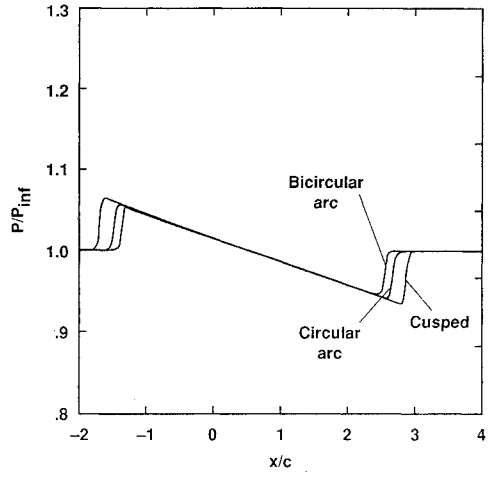

Fig. 9 Shock waves at $y = 19.3c$ showing effect of geometry on the far-field N wave, Mach number = 1.414.

that the bicircular airfoil has the shortest signature and the cusped (shockless) airfoil the longest. Presumably, the two shocks interact with greater vigor and drive the pressure peaks to a lower value as the wave enters the asymptotic region.

Conclusions

A new derivation of the adiabatic two-dimensional Euler equations using eigenfunction analysis showed a Burgers equation model can be used to predict the flow to second order. Computational results indicate that asymptotic N waves form rather quickly. This analysis illustrates the close relationship between supersonic aerodynamics and nonlinear acoustics and the use of aeroacoustic numerical tools to solve this steady flow problem.

An analysis of the midfield region similar to that just described would be a very useful design tool for sonic-boom tradeoff studies. Both nonlinear and three-dimensional azimuthal effects in the midfield that are not accounted for in ray theory may be significant factors in reducing the detrimental effects of sonic booms. Further work is continuing in this direction.

References

[1]Carlson, H. W., and Maglieri, D. J., "Review of Sonic Boom Generation and Prediction Methods," *Journal of the Acoustical Society of America*, Vol. 51, No. 2, 1972, pp. 675–685.

[2]Davis, S. S., "Calculation of Sonic Boom Signatures by Bicharacteristic Methods," *AIAA Journal*, Vol. 10, No. 9, 1973, pp. 1211–1215.

[3]Whitham, G. B., "The Flow Pattern of a Supersonic Projectile," *Communications on Pure and Applied Mathematics*, Vol. V, 1952, pp. 301–348.

[4]Walkden, F., "The Shock Pattern of a Wing-Body Combination Far From the Flight Path," *Aero Quarterly*, Vol. 9, May 1958, pp. 164–194.

[5]Cheung, S. H., Edwards, T. A., and Lawrence, S. L., "Application of Computational Fluid Dynamics to Sonic Boom Near- and Mid-Field Predictions," *Journal of Aircraft*, Vol. 29, Sept./Oct. 1992, pp. 920–926.

[6]Hayes, W., and Runyan, H., "Sonic Boom Propagation through a Stratified Atmosphere," *Journal of the Acoustical Society of America*, Vol. 51, No. 2, 1972, pp. 695–701.

[7]Van Dyke, M., *Perturbation Methods in Fluid Mechanics*, Parabolic Press, Stanford, CA, 1975, p. 107.

[8]Cole, J. D., *Perturbation Methods in Applied Mathematics*, Blaisdell, Waltham, MA, 1968, pp. 227–238.

[9]Landau, L. D., and Lifshitz, E. M., *Fluid Mechanics*, Pergamon, London, 1959, pp. 399–405.

[10]Davis, S. S., "Low Dispersion Finite Difference Methods for Acoustic Waves in a Pipe," *Journal of the Acoustical Society of America*, Vol. 90, Nov. 1991, pp. 2775–2781.

[11]Lighthill, M. J., "Higher Approximations," *General Theory of High Speed Aerodynamics*, edited by W. R. Sears, Princeton Univ. Press, 1954, pp. 386 and 398.

[12]Davis, S. S., "A Space-Time Discretization Procedure for Wave Propagation Problems," NASA TM 102215, Nov. 1989.

[13]Augenbaum, J., "An Adaptive Pseudospectral Method for Discontinuous Problems," *Applied Numer. Math*, Vol. 5, Oct. 1989, pp. 459–480.

[14]Nessyahu, H., and Tadmor, E., "Non Oscillatory Central Differencing for Hyperbolic Conservation Laws," *Journal of Computational Physics*, Vol. 87, 1990, pp. 408–463.

[15]Whitham, G. B., *Linear and Nonlinear Waves*, Wiley, New York, 1974, p. 108.